MATERIALS CHEMISTRY
FRONTIERS

RESEARCH ARTICLE

View Article Online
View Journal | View Issue

Cite this: *Mater. Chem. Front.*, 2021, **5**, 7628

Triethyl phosphate in an antisolvent: a novel approach to fabricate high-efficiency and stable perovskite solar cells under ambient air conditions†

Pengyun Zhang,[a] Ningxia Gu,[a] Xiang Chen,[a] Lixin Song,*[a] Pingfan Du,[a] Wei-Hsiang Chen[b] and Jie Xiong*[a]

Organometallic halide perovskite solar cells (PSCs) with a high power conversion efficiency (PCE) have attracted immense attention for applications and commercialization. Nevertheless, it is still a challenge to find a novel method to overcome the rapid degradation of the perovskite so that PSCs demonstrating an excellent performance can be fabricated in an ambient environment without a glove box. Herein, in this paper, triethyl phosphate (TEP) is introduced into the perovskite layer *via* antisolvent engineering to serve as a crystallization aid and a humidity stabilizer. Impressively, the electron-rich phosphate group in TEP can form a strong chemical bonding interaction with the perovskite (Pb–O) to passivate the defects produced during crystallization. More interestingly, the ethyl group with its hydrophobic effect can protect the perovskite film from corrosion by the moisture in the air. As a result, the TEP-modified perovskite film demonstrates a dense and defectless morphology with a large grain size (a maximum of more than 1 μm). The TEP-treated device achieves a dramatic efficiency of 19.6% and negligible hysteresis of the photocurrent. Moreover, the humidity resistance of the TEP-modified device is significantly enhanced. The normalized PCE of the TEP-modified device (unencapsulated) can still retain 82% of its initial value after being stored in an 85% humidity environment under dark conditions for 400 hours. This finding provides a promising approach for facilitating the commercialization of PSCs.

Received 8th May 2021,
Accepted 20th August 2021

DOI: 10.1039/d1qm00680k

rsc.li/frontiers-materials

1. Introduction

The power conversion efficiency (PCE) of laboratory-scale organic–inorganic halide perovskite solar cells (PSCs) has dramatically exceeded 25% within ten years of their first report.[1–4] Such a rapid development is due to the excellent photovoltaic performance of organo-lead halide perovskites *via* their high carrier mobility and optical absorption.[5,6]

Despite the excellent photovoltaic properties achieved by PSCs at the laboratory scale, the perovskite material decomposes in the presence of air, especially at high temperatures and under humid conditions. Therefore, high-efficiency perovskites are usually prepared in inert environments, which are expensive and inconvenient for scale-up purposes. Furthermore, the solution-based fabrication processes for perovskite films lead to formation of abundant defects and traps at the grain boundaries (GBs), especially at the surfaces. These defect sites are more reactive toward oxygen and H_2O in air environment, resulting in the degradation of the perovskite. Hence, the crucial instability issues of PSCs under realistic operation conditions still need to be overcome for commercial applications.[7,8]

Recently, a lot of progress in improving the photovoltaic performance and stability of devices has been achieved using various modification engineering approaches, such as composition engineering,[9,10] interface engineering,[11,12] additive engineering,[13,14] and solvent engineering.[15,16] These methods ameliorate the morphology, charge-transport ability and long-term stability of the perovskite, consequently enhancing the efficiency and stability of the PSCs. Moreover, it has been found that the uncoordinated Pb sites at the surface can be effectively passivated by a Lewis base or an electron donor, such as thiophene,[17] lead salts,[18] diethyl ether,[19] and urea,[20] through chemical interactions that can saturate the lead coordination sphere to control the reaction and nucleation processes of the perovskite grains. However, in most of these reports, the devices were fabricated in a nitrogen-filled glove box, which is expensive as well as impractical for industrial manufacturing. Hence, finding a way to fabricate high-efficiency PSCs with good

[a] *College of Textile Science and Engineering, Zhejiang Sci-Tech University, Hangzhou, 310018, China. E-mail: lxsong12@zstu.edu.cn, jxiong@zstu.edu.cn*
[b] *School of Science, Huzhou University, Huzhou, 313000, Zhejiang, China*

† Electronic supplementary information (ESI) available. See DOI: 10.1039/d1qm00680k

stability under ambient conditions and without a glove box is essential for their applications.

In this contribution, the above goal is realized *via* introducing triethyl phosphate (TEP) into a perovskite through an antisolvent. In particular, we use ethyl acetate (EA), which shows quick volatilization and good miscibility with TEP as the anti-solvent, to accelerate the supersaturated state during the perovskite crystal-formation process.[21–23] At a suitable time point, the electron-rich TEP in the antisolvent is added dropwise onto the $CH_3NH_3PbI_3$ precursor film forming top seeds, and these top perovskite seeds can act as nuclei for promoting the growth of large grains with higher crystallinity. On the other hand, the electron-rich phosphate group (mainly oxygen) can form a powerful chemical bonding interaction with the perovskite (mainly lead) to passivate the defects and traps formed during crystallization. Furthermore, the ethyl groups, with a hydrophobic effect, and where the hydrophobic parameter calculation reference value ($X\log P$) of TEP is a positive value greater than zero (0.8), can serve as an ''umbrella'' for safeguarding the perovskite grains from erosion by the humidity in the ambient air. Consequently, the TEP-modified perovskite film displays a flat, smooth and defect-free morphology with large-dimensional grains (with a maximum of more than 1 μm). This can significantly enhance the light-absorption capacity and short-circuit current value of PSCs. Moreover, the passivated defects and traps at the surface and the GBs caused by the addition of TEP can remarkably improve the photovoltaic performance, particularly the open-circuit voltage (V_{oc}), of the device. The optimized PSCs bring about a dramatic 19.6% PCE and indicate negligible hysteresis of the photocurrent. In addition, the moisture stability of the TEP-modified perovskite film is significantly enhanced and the normalized efficiency of the TEP-modified unencapsulated device still retains 82% of its initial value. Overall, this simple, effective and low-priced approach for fabricating high-efficiency PSCs with good stability in an air environment without a glovebox advances their preparation and commercialization.[24]

2. Experimental methods

2.1. Materials

Fluorine-doped tin oxide (FTO)-etched glass substrates were purchased from Advanced Electronic Technology Co., Ltd. A solution of titanium diisopropoxide bis(acetylacetonate) (75 wt% in isopropanol) was purchased from Sigma-Aldrich. The perovskite materials (PbI_2 and CH_3NH_3I) were purchased from Kunshan Sunlaite New Energy Technology Co., Ltd. Triethyl phosphate (TEP) was purchased from Shanghai Macklin Biochemical Technology Co., Ltd. 2,2′,7,7′-Tetrakis(*N*,*N*-di-*p*-methoxyphenylamine)-9,9′-spirobifluorene (Spiro-OMeTAD) powder was purchased from Xi'an Polymer Light Technology Corporation. Other materials were supplied by Aladdin Reagent (Shanghai) Co., Ltd.

2.2. Device fabrication

The FTO-etched glass substrates were cleaned by ultrasonic treatment with acetone, ethyl alcohol and isopropyl alcohol for 30 minutes, respectively. After drying at 120 °C, the substrates were treated with ultraviolet (UV) ozone for 25 minutes to eliminate the organic compounds on the surface of FTO-etched glass. Later, TiO_2 solution was spin-coated onto the FTO-etched substrate as the electron-transport layer (ETL). After increasing the temperature to 450 °C at 5 °C min^{-1}, the substrate was continuously annealed for 35 minutes. Then the perovskite precursor solution was spin-coated onto the TiO_2 layer at 2000 rpm (revolutions per minute) for 15 s and 4000 rpm for 20 s in turn. Specifically, ethyl acetate (EA, with or without TEP) was used as the anti-solvent in the production process, and the schematic diagram is clearly presented in Fig. S1 (ESI†). After the substrate had been annealed at 100 °C for 40 minutes, the solution of Spiro-OMeTAD was spin-coated onto the perovskite layer at 4500 rpm for 25 s. In the last step, a thickness of approximately 60 nm of Ag as the electrode was deposited by thermal evaporation on the top. Notably, high-efficiency and stable perovskite solar cells were prepared entirely under ambient conditions (RH ≈ 50%) without a glove box, hence greatly reducing the manufacturing costs.

2.3. Characterization

The morphology of the perovskite ($CH_3NH_3PbI_3$) films was obtained *via* scanning electron microscopy (SEM, Ultra55, ZEISS). The elemental orbitals were analyzed using X-ray photoelectron spectroscopy (XPS, K-Alpha). Fourier transform infrared spectroscopy (FTIR, Nicolet 5700) measurements were obtained in transmittance mode. The absorption spectra were measured using a UV-Visible spectrophotometer (UV-Vis, Lambda 900). The crystal structures of the $CH_3NH_3PbI_3$ ($MAPbI_3$) films were studied using X-ray diffraction (XRD, Thermo ARL-X′TRA) with Cu Kα radiation (λ = 1.5418 Å). Transient-state photoluminescence (PL) and time-resolved photoluminescence (TRPL) were studied using a PG2000-Pro-EX spectrophotometer (Shanghai Ideaoptics Corporation) and a transient fluorescence spectrometer (FLS980, Edinburgh Instruments), respectively. The current density–voltage (J–V) characteristics of the PSCs were studied using a source meter (Keithley 2400-SCS) under AM 1.5 illumination with an intensity of 100 mW cm^{-2}. Electrochemical impedance spectroscopy (EIS) was investigated using an electrochemical workstation (Zennium Pro). Water-contact-angle images of the $MAPbI_3$ films were recorded using a contact-angle instrument (Krüss Optronic).

3. Results and discussion

To significantly reduce the traps and defects of the perovskite film at the surface and grain boundaries (GBs), herein we introduce an economical, effective and hydrophobic electron-rich organophosphorus ligand, triethyl phosphate (TEP), into the $CH_3NH_3PbI_3$ ($MAPbI_3$) film as a defect passivator and a morphology-modifying agent. In the perovskite film fabrication process, ethyl acetate (EA) solution with the addition of TEP was added dropwise from above as displayed in Fig. 1a. Then, the electron-rich TEP on top of the $MAPbI_3$ precursor could

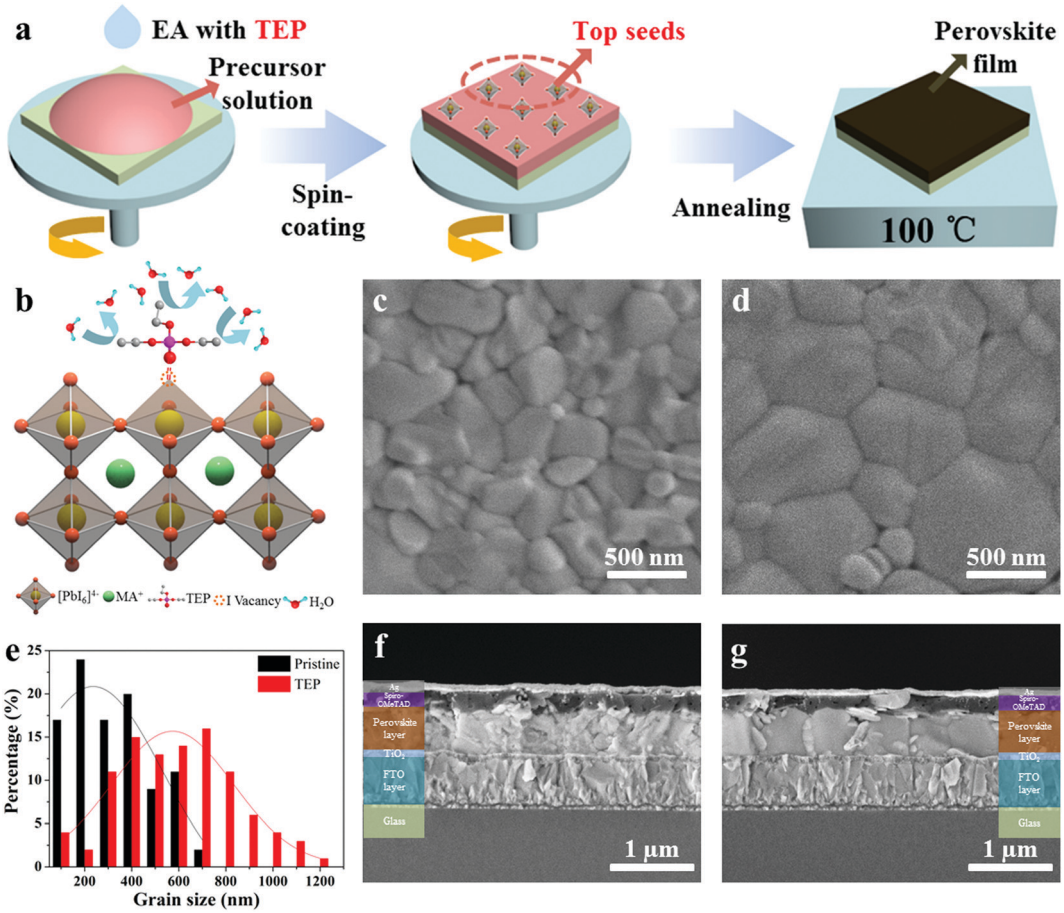

Fig. 1 (a) Illustration of top seeds and the annealing method. (b) Schematic illustration of defect-passivation between triethyl phosphate (TEP) and the undercoordinated Pb^{2+} ion. The hydrophobic nature of TEP can effectively resist erosion by H_2O in the air environment. (c and d) Top-view SEM images of perovskite films without and with 3 vol% TEP, respectively. (e) Histogram of the grain size distribution of both perovskite films. (f and g) Cross-section SEM images of pristine PSC and the TEP-modified perovskite-based device, respectively.

react faster with the perovskite (especially Pb^{2+}) than the pristine sample and help the antisolvent to take away some precursor solvent at the same time. After that, the TEP-modified perovskite quickly generates many small crystals at the top of the film. Finally, the initially produced perovskite small crystals cluster and form top seeds, and these top perovskite seeds can act as the nuclei for promoting the growth of large grains with higher crystallinity. The chemical structure of TEP is demonstrated in Fig. S2 (ESI†) and consists of three ethyl functional groups at three of the vertices and an independent oxygen atom at the fourth vertex. TEP can be used as a crystallization-inducing reagent.[25] Fig. S3 (ESI†) shows the optical images of both perovskite films without and with the top perovskite seeds, and these samples underwent the spin-coating step (before heat treatment). The color of the perovskite film deepens after TEP doping, illustrating the emergence of some perovskite seeds. Furthermore, Fig. 1b indicates the schematic illustration of defect-passivation between TEP and the undercoordinated Pb^{2+} ion. As the anti-solvent with TEP was added dropwise from above during the perovskite spin-coating process to assist crystallization, the electron-rich phosphate group can form a powerful interaction with the under;coordinated Pb^{2+} ion, simultaneously filling the iodide vacancy at the surface. This strong interconnection effectively passivates the defects and traps of the perovskite film, especially at the surface, to obtain a uniform perovskite film for further improvement of the PCE and the stability of the ensuing PSC. Besides, the hydrophobic nature of the ethyl group in TEP can effectively resist erosion by H_2O during fabrication in an air environment.

To verify these suppositions, top-view SEM measurements were performed and are demonstrated in Fig. 1c and d. Generally, when the $MAPbI_3$ film is fabricated in air (under high-humidity conditions), the surface of the perovskite film commonly has numerous defects and pinholes with many small grains, as illustrated in Fig. 1c. By contrast, when a suitable concentration (3 vol%) of TEP is added to the perovskite film, the modified film shows a dense, flat, smooth and defectless morphology with larger sized grains (with a maximum of more than 1 μm), fewer GBs and preferable surface coverage, as displayed in Fig. 1d. The main reason is that a favorable amount of TEP with plentiful electron donors can suppress the morphological defect formation and fill the I^- vacancies to assist crystallization of the perovskite grains during fabrication.[26–28] Notably,

the preparation parameters of the two kinds of perovskite film, such as the spin-coating speed and the relative humidity (RH), are exactly the same except for the presence or absence of TEP. These results reveal the greater defect passivation and morphology modulation of the TEP-modified perovskite film. The grain size distribution histogram of both perovskite films is illustrated in Fig. 1e. The larger grain size and passivated GBs of the TEP-modified perovskite film are crucial for a higher performance and stability of the resulting devices.

Moreover, for testing the effects of different concentrations of TEP on the perovskite film, the top-view SEM images of perovskite films doped with different concentrations of TEP and the corresponding histogram of the grain size distribution are shown in Fig. S4 (ESI†). The perovskite film shows a considerably compact and flat morphology with larger crystal grain sizes and fewer defects *via* the addition of a small amount of TEP (1 vol%), as indicated in Fig. S4a (ESI†). However, as the concentration of the TEP is continuously increased to 5 vol%, the perovskite film becomes defective at the GBs and shows some small grains, which seriously weaken the improvement of the device performance, as indicated in Fig. S4b (ESI†). Therefore, the optimal concentration of TEP is 3 vol%. Apart from the surface morphology of the perovskite film, the high-quality cross-sectional completeness also plays a critical role in the photovoltaic performance of PSCs. Hence, a cross-sectional SEM analysis of the PSCs was carried out and the results are shown in Fig. 1f and g. The grains of the pristine perovskite film are small and fragmented with lots of pinholes and cracks. By contrast, the TEP-modified perovskite film indicates integral and quasi-all-in-one grains with dense GBs. In particular, the thickness (about 500 nm) of the perovskite film did not change noticeably after the addition of TEP, and the other layers of two PSCs are identical. This implies that the higher cross-sectional quality of the TEP-modified perovskite layer is also caused *via* the addition of TEP, and the better cross-sectional morphology can result in a higher performance and better stability for the PSCs.[29,30]

For confirming the change in surface composition of the perovskite films after TEP modification, the Pb 4f core level spectra of perovskite films with/without TEP were investigated using high-resolution X-ray photoelectron spectroscopy (XPS), as revealed in Fig. 2a. The dominant features of Pb $4f_{5/2}$ and Pb $4f_{7/2}$ are located at 143.08 eV and 138.18 eV, respectively. After introducing TEP, the Pb $4f_{5/2}$ and Pb $4f_{7/2}$ peaks clearly shift to lower binding energies at 142.77 eV and 137.87 eV. Such 0.31 eV shifts suggest the coordination between TEP and the Pb^{2+} ion with the increasing electron density of the Pb atomic nucleus.[31–33] Moreover, the unsaturated Pb signals of the pristine perovskite film at 141.31 eV and 136.43 eV are certainly suppressed in the TEP-modified perovskite film, which directly confirms the interaction between lead and oxygen.[34–36] Furthermore, the XPS survey spectra of the perovskite films (with/without TEP) are revealed in Fig. S5 (ESI†). Fourier transform infrared spectroscopy (FTIR) is employed to evaluate the bonding information of TEP and the perovskite, as displayed in Fig. 2b. The peak at 573 cm^{-1} is assigned to the Pb–O symmetric bending vibration and a low-intensity peak can be observed in the pristine film, which probably results from the adsorption of oxygen during fabrication under ambient conditions.[37] Obviously, a higher-intensity peak at the same wavelength can be observed in the TEP-modified perovskite film. Such a direct enhancement reveals that oxygen in TEP possibly interconnects with the Pb positive ions in the perovskite through a Lewis acid–base reaction. These results provide powerful evidence for the proposals indicated in Fig. 1a and b.

It is well known that the better absorbance of a perovskite film can directly improve the short-circuit current (J_{sc}) of a PSC. Therefore, the ultraviolet visible (UV-Vis) spectra of two kind perovskite films were studied and shown in Fig. 3a. Obviously, a clear absorption peak located at about 758 nm in the spectra. Notably, the thickness of each of the perovskite layers is about 500 nm, and the main reason for this significantly improved light-harvesting capacity is the higher quality (enlarged grain size) of the TEP-modified perovskite film, as exhibited in Fig. 1d and g.[38,39] Moreover, the UV-Vis spectra of perovskite films modified with various TEP concentrations are presented in Fig. S6 (ESI†). Apparently, the optimized absorbance of the perovskite film can be observed *via* the addition of a small amount of TEP (1 vol%). However, excessive addition leads to a decreased absorbance, which accords with the SEM outcomes,

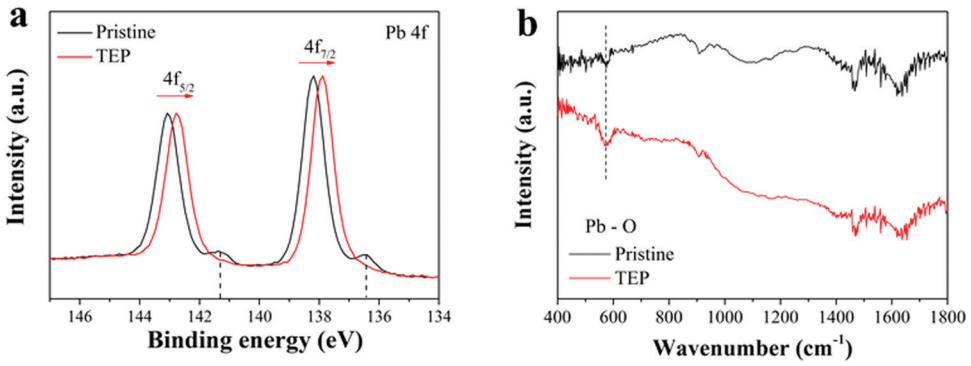

Fig. 2 (a) XPS spectra of the Pb 4f core level of the perovskite films (without and with TEP). (b) FTIR spectra of the pristine and TEP-modified perovskite films.

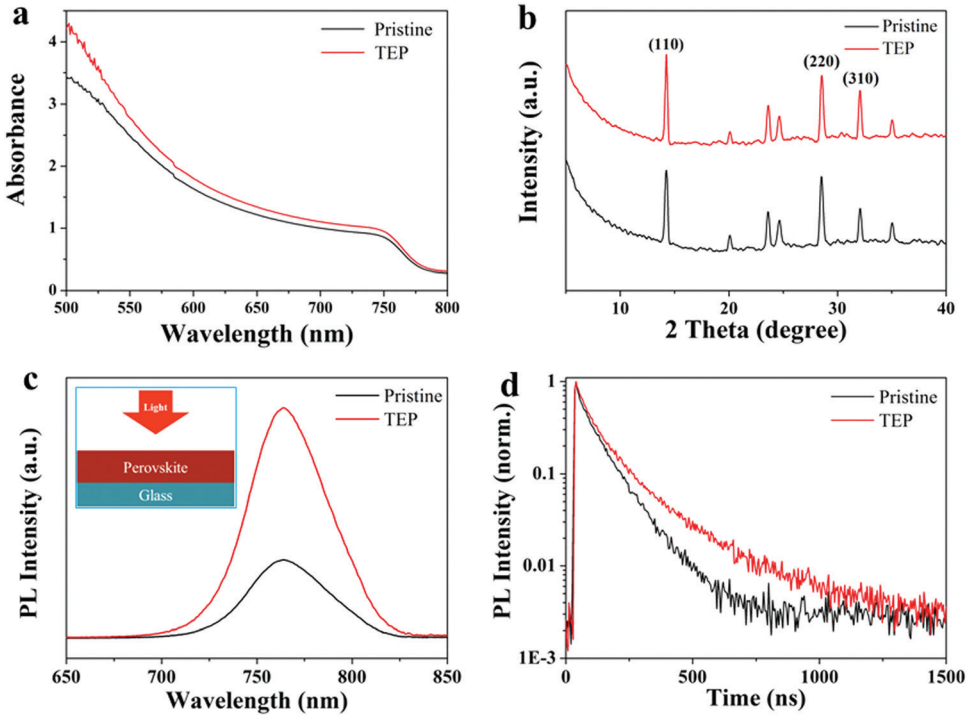

Fig. 3 (a) UV-Vis absorbance spectra and (b) XRD analysis of the pristine and TEP-modified perovskite films. (c and d) PL spectra and TRPL characteristics, respectively, of the pristine and TEP-modified perovskite films. The inset in (c) shows the structure of the tested samples.

as shown in Fig. S4b (ESI†). In addition, the crystallinity of the perovskite layers was carefully examined using XRD and the patterns are exhibited in Fig. 3b. These indicate that the peaks at 14.2°, 28.6° and 32.1° correspond to reflections from the (110), (220), and (310) planes of the orthorhombic space group (*I*4/*mcm*), respectively. Moreover, the full-width at half maximum (FWHM) of the (110) plane in the TEP-modified perovskite (0.25°) is narrower than that of the pristine film (0.31°) and the intensity is stronger, as displayed in Fig. S7 (ESI†), indicating that the crystallization of the perovskite is improved.[40] The main reason for this optimization is that the addition of TEP *via* spin-coating can passivate defects produced during the perovskite film formation, as shown in Fig. 1a and b.

Fig. 3c exhibits the PL spectra of the two samples to evaluate the charge-carrier recombination dynamics of the perovskite film without or with TEP. It can be observed that the PL intensity of the TEP-modified perovskite film is significantly improved compared with that of the pristine film. This obvious PL enhancement provides powerful evidence of the suppressed non-radiative recombination.[41,42] For investigating the photoelectric properties further, the time-resolved PL (TRPL) decay of the two perovskite films is studied. As revealed in Fig. 3d, the TEP-modified $CH_3NH_3PbI_3$ film demonstrates a longer non-radiative charge-decay lifetime, suggesting the reduction in the trap-mediated bulk or surface recombination and realization of a higher transport capability during the device operation. The fitted parameters of the TRPL spectra are provided in Table 1. All experimental data can be well fitted to the biexponential decay function $I(t) = I_0 + A_1 e^{(-t-t_0/\tau_1)} + A_2 e^{(-t-t_0/\tau_2)}$. Here A_1 and A_2 are the decay amplitudes, τ_1 is related closely to non-radiative recombination and τ_2 is the component of radiative recombination from the perovskite.[43] Furthermore, the average decay lifetime can be obtained from the equation $\tau_{avg} = \left(\sum_i A_i\tau_i^2 \Big/ \sum_i A_i\tau_i\right)$. The TRPL results indicate that the high quality of the TEP-modified perovskite film can decrease the trap-assisted recombination and thus increase the average decay lifetime from 85.61 ns to 144.74 ns. This suppressed non-radiative recombination can result in a lower energy loss and thus increase the open-circuit voltage (V_{oc}) of the resulting PSC.[44]

Table 1 Fitted parameters of TRPL spectra for the pristine and TEP-modified perovskite films

Samples	A_1 (%)	τ_1 (ns)	A_2 (%)	τ_2 (ns)	τ_{avg} (ns)
Pristine	36	10.67	64	90.58	85.61
TEP	29	37.72	71	155.35	144.74

To assess the performance of the TEP-modified perovskite film-based devices, the photovoltaic properties of the PSCs, measured *via* the *J*–*V* curve and the hysteresis, are plotted in Fig. 4a and b. Fig. 4a shows the *J*–*V* curves recorded in both the forward and reverse scan directions at the same scan rates. Table 2 lists all the photovoltaic parameters of the two devices, and there is no obvious hysteresis (H = 0.038) of the photocurrent observed for the TEP-doped perovskite-based PSC upon changing the sweep direction. In addition, the hysteresis (H) index is defined by the equation $H = \frac{\text{PCE reverse} - \text{PCE forward}}{\text{PCE reverse}}$.

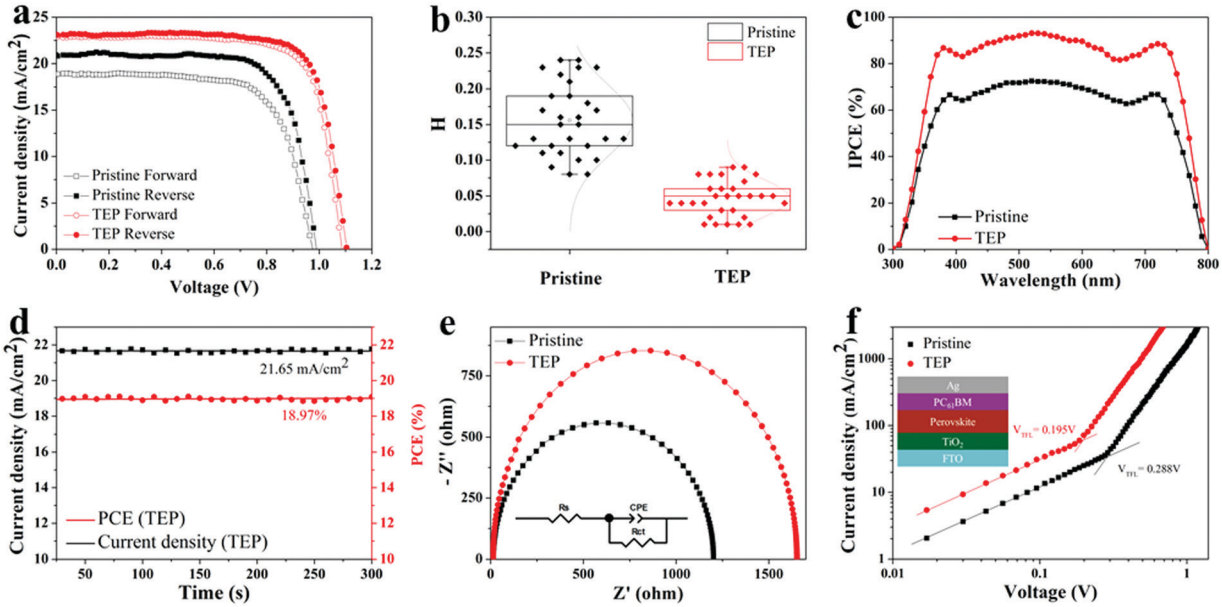

Fig. 4 (a) Typical *J*–*V* characteristics of two PSCs with different scan directions. (b) Statistics of the *H* index in 30 sets of PSCs to quantify the hysteresis of the devices. (c) IPCE spectra of pristine and TEP-modified PSCs. (d) Maximal steady-state photocurrent and stabilized PCE of optimal TEP-treated devices. (e) Nyquist plots at *V* = 0.9 V bias of pristine and TEP-modified PSCs under dark conditions. (f) Dark *J*–*V* curves of electron-only PSCs with the structure of FTO/TiO_2/$MAPbI_3$/$PC_{61}BM$/Ag (as shown in the inset).

Moreover, detailed information on the *J*–*V* hysteresis for 30 PSCs of different batches is demonstrated in Fig. 4b. The lower hysteresis index demonstrates the effective passivation of defects and the narrower deviation between the devices shows the better reproducibility of the TEP-modified PSCs.[45] The enhanced perovskite film quality with uniform surfaces and GBs can effectively suppress the surface charge-trap states and simultaneously strengthen the charge transport of the device, and these are the cause of the reduced hysteresis.[46] It is confirmed that the champion PCE of the TEP-modified PSC reaches 19.6%, with the J_{sc}, V_{oc} and fill factor (FF) all being remarkably improved; however, the PCE of the pristine device yields only 15.2%. Furthermore, the *J*–*V* curves of the PSCs doped with various TEP concentrations are shown in Fig. S8 (ESI†) and the photovoltaic parameters are summarized in detail in Table S1 (ESI†). After doping with a small amount of TEP, the PCE of the devices is enhanced. However, the photovoltaic performance of the PSCs decreases because of the poor perovskite film quality and the low light absorbance, which are caused by an excess of TEP. In addition, 30 individual devices of all kinds of PSCs were also studied to check the statistical distribution and repeatability of the PCE, as exhibited in Fig. S9 (ESI†). The PSCs based on the TEP-modified perovskite clearly display an enhancement in both the efficiency and the repeatability, which accords with the reduced non-radiative recombination and improved electron–hole recombination resistance. Fig. 4c reveals the external incident-photon-conversion efficiency (IPCE) spectra of PSCs without and with TEP. The improved IPCE of the TEP-modified device is mainly due to the higher film quality and better light absorption, as exhibited in Fig. 3a. To examine the steady output of the optimal TEP-treated device, the stabilized PCE and the maximum steady-state photocurrent are measured under a maximum power point of 0.92 V for 300 s, as shown in Fig. 4d. It is clear that the current density curve of the TEP-treated PSC is stabilized at 21.65 mA cm^{-2} with the corresponding stabilized PCE being at 18.97%. Moreover, the maximal steady-state photocurrent and the stabilized PCE of the pristine device are exhibited in Fig. S10 (ESI†). The lower stabilized PCE and the photocurrent are consistent with the *J*–*V* characteristics.[47]

Table 2 Detailed photovoltaic parameters of both devices in different scan directions

Samples	J_{sc} (mA cm^{-2})	V_{oc} (V)	FF (%)	PCE (%)
Pristine forward	18.90	0.97	70.58	12.94
Pristine reverse	20.81	0.98	74.53	15.20
TEP forward	22.86	1.08	76.35	18.85
TEP reverse	23.08	1.10	77.20	19.60

For investigating the trap-assisted recombination phenomena and the charge-transfer performance of the PSCs, electrochemical impedance spectroscopy (EIS) measurements were carried out, as shown in Fig. 4e. The inset shows the equivalent circuit model composed of the charge-transfer resistance (R_{ct}) and the series resistance (R_s). As is well known, R_s is the series resistance that includes the contact wires and materials. The combination of the R_{ct} and the CPE relates to the high-frequency arc in the impedance spectrum, which is associated with the charge-transport resistance at the heterojunction interface and the associated capacitance.[48] Table 3 lists the corresponding parameters of the equivalent circuits. A lower R_s and a higher R_{ct} are achieved for the TEP-modified device, revealing the more efficient charge transfer at the interfaces of the PSC. These results confirm that interfacial combination is significantly suppressed by applying TEP, and the

Table 3 Detailed fitting of internal series resistance (R_s), the electron–hole recombination resistance (R_{ct}) and the electron trap density (N_{trap}) of the two kinds of PSC

Samples	R_s (Ω)	R_{ct} (Ω)	V_{TFL} (V)	N_{trap} (cm^{-3})
Pristine	14.7	1201.9	0.288	3.67×10^{15}
TEP	12.8	1651.8	0.195	2.49×10^{15}

suppressed electron–hole recombination can efficiently improve the V_{oc} of PSCs. To understand the defect states of PSCs more deeply, space charge limited current (SCLC) measurements are obtained and are demonstrated in Fig. 4f. The density of trapping states (N_{trap}) is recorded by dark J–V curves in electron-only devices. The defect density is calculated from the following equation: $N_{traps} = \frac{2\varepsilon\varepsilon_0 V_{TFL}}{eL^2}$, where ε, ε_0, L and V_{TFL} are the vacuum permittivity, the relative dielectric constant (~28.8), the thickness of the perovskite film (~500 nm) and the trap-filling limit voltage, respectively.[49] It can be estimated that the N_{trap} value is impressively reduced from 3.67×10^{15} cm^{-3} for the pristine device to 2.49×10^{15} cm^{-3} for the TEP-modified PSC. The detailed parameters are summarized in Table 3. The complete spectrum (including the ohmic region, the trap-filling region and the child region) is displayed in Fig. S11a (ESI†)[50] and the meaningful statistical collection of data on 30 sets of samples from electron-only devices is shown in Fig. S11b (ESI†). The TEP-based devices have lower N_{trap} values and show a smaller deviation, which indicates their better quality and reproducibility. Moreover, the hole-only samples were measured and the results are shown in Fig. S12 (ESI†). It is deduced that the TEP-treated device shows a lower trap recombination and defect density than the pristine device, mainly on account of the passivated GBs, the improved perovskite surface morphology and enhanced interface features of the TEP-modified perovskite film.[51] Besides, the effective charge transport contributes to the higher FF value of the resulting PSCs.

In addition to the outstanding photovoltaic performance, an excellent moisture resistance of the perovskite film is a crucial issue for applicability, especially for commercialization of the PSCs. In order to study the role of TEP in the humidity stability of the perovskite, perovskite films with and without TEP were placed under 85% RH conditions in the dark for different time periods, as shown in Fig. 5a. The pristine film showed rapid degradation after 100 hours and degraded to PbI_2 at the edges after 400 h. By contrast, the perovskite film that was protected by TEP showed no significant change. Furthermore, the perovskite films that were placed under 85% RH conditions for 400 hours in the dark were carefully investigated using XRD, as demonstrated in Fig. 5b. The experimental results display that a clear PbI_2 signal could be detected in the pristine perovskite film. However, there is no obvious PbI_2 peaks could be observed in the XRD analysis of the TEP-modified perovskite film. These outcomes imply that defect passivation and the hydrophobic properties of TEP can effectively defend the perovskite film from erosion by moisture in an air environment. Moreover, the insets of Fig. 5c indicate that the water-contact-angle of the perovskite films increases from 65.55° (pristine) to

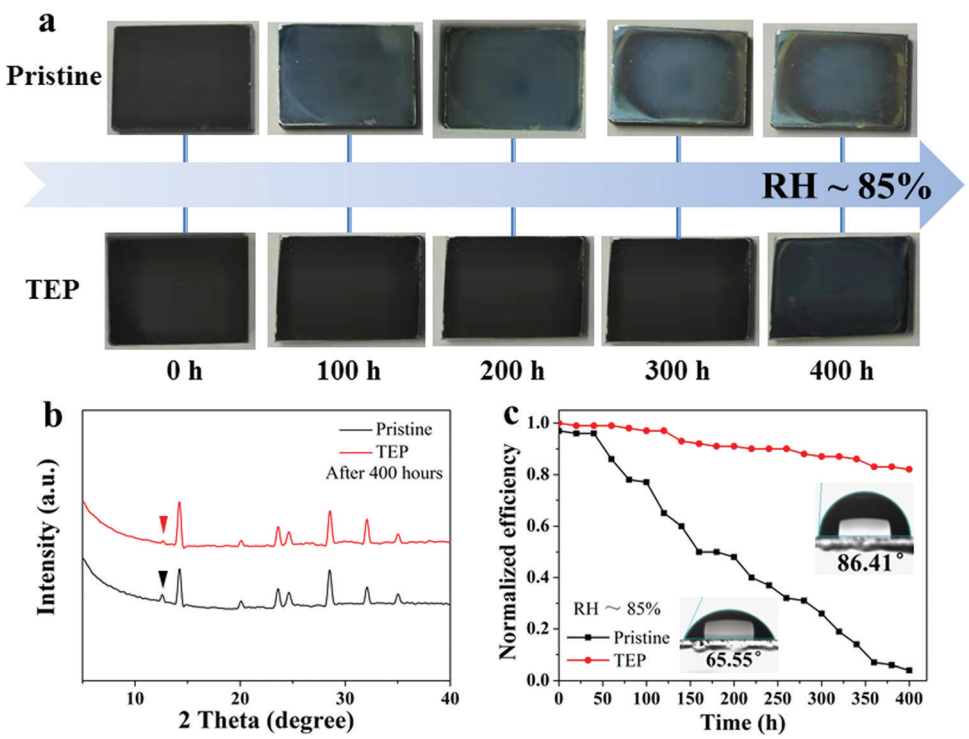

Fig. 5 (a) Photographs of perovskite films without and with the TEP additive stored under dark conditions at RH ≈ 85% for different time periods. (b) XRD analysis of perovskite films stored under dark conditions at RH ≈ 85% for 400 hours. (c) Normalized PCE recorded under room temperature, RH ≈ 85%, dark conditions for 400 hours. The insets show the water-contact-angle of the pristine and TEP-modified perovskite films.

86.41° (TEP-modified). The larger angle of the TEP-modified $MAPbI_3$ film indicates its improved moisture resistance ability. These significant enhancements are in accord with the mechanism exhibited in Fig. 1b. For surveying the humidity resistance of the devices, the normalized efficiency is shown in Fig. 5c. After the non-encapsulated PSCs were placed under 85% humidity conditions for 400 hours in the dark, the normalized PCE of the TEP-modified device still maintained 82% of its initial value, which is better than that of the pristine device, which retained just 4%. Therefore, high-quality perovskite films can be realized using the electron-rich and hydrophobic TEP, which further enhances the efficiency and long-term stability of the resulting device, consequently advancing the commercialization of PSCs.[52–54]

4. Conclusions

In conclusion, a novel approach to fabricate high-efficiency and stable perovskite solar cells in an air environment without a glove box is achieved *via* introducing triethyl phosphate into the perovskite. First, the electron-rich TEP on top of the $MAPbI_3$ precursor film forms top seeds, and these top perovskite seeds can act as nuclei for promoting the growth of large grains with higher crystallinity. On the other hand, the electron-rich phosphate group can form a powerful chemical bonding interaction with the perovskite to passivate the traps and defects produced during crystallization. Finally, the ethyl groups with a hydrophobic effect of TEP serve as an ''umbrella'' for preserving the perovskite film from corrosion by the surrounding humidity. As a result, the TEP-modified perovskite film shows a flat and defectless morphology with large grains (with a maximum size of more than 1 μm). The passivated surface traps and ideal surface coverage caused by TEP could significantly enhance the photovoltaic performance of the resulting PSCs. The optimized device realizes a dramatic PCE of 19.6% and with negligible hysteresis of the photocurrent. Furthermore, the moisture stability of the TEP-modified device is significantly improved. The TEP-modified perovskite film reveals no obvious degradation that can be detected using XRD after the film has been stored under dark conditions at 85% RH for 400 hours. The normalized PCE of the TEP-modified device (unencapsulated) can still retain 82% of its initial value after being stored under dark conditions at RH = 85% for 400 hours. Considering the above, this contribution provides a practical approach for facilitating the commercialization of PSCs prepared using a low-cost, hydrophobic additive and *via* a simplified fabrication method.

Author contributions

Pengyun Zhang: investigation, formal analysis, and writing – original draft. Ningxia Gu: data curation, and methodology. Xiang Chen: validation. Lixin Song: supervision, and writing – review and editing. Pingfan Du: funding acquisition. Wei-Hsiang Chen: conceptualization, and software. Jie Xiong: funding acquisition, and project administration.

Conflicts of interest

The authors declare no competing financial interests.

Acknowledgements

The financial support for this work is provided by the Zhejiang Provincial Natural Science Foundation of China (LQ19E030020, LY21F040008); Foundation of Zhejiang Educational Committee (Y201840334); the Fundamental Research Funds of Zhejiang Sci-Tech University (2021Q001); and the Applied Basic Research Project of China National Textile and Apparel Council (J201801).

References

1 A. Kojima, K. Teshima, Y. Shirai and T. Miyasaka, Organometal Halide Perovskites as Visible-Light Sensitizers for Photovoltaic Cells, *J. Am. Chem. Soc.*, 2009, **131**, 6050.
2 S. J. Lee, S. S. Shin, J. Im, T. K. Ahn, J. H. Noh, N. J. Jeon, S. I. Seok and J. Seo, Reducing Carrier Density in Formamidinium Tin Perovskites and Its Beneficial Effects on Stability and Efficiency of Perovskite Solar Cells, *ACS Energy Lett.*, 2017, **3**, 46–53.
3 H.-A. Lin, N. Mitoma, L. Meng, Y. Segawa, A. Wakamiya and K. Itami, Hole-transporting materials based on thiophene-fused arenes from sulfur-mediated thienannulations, *Mater. Chem. Front.*, 2018, **2**, 275–280.
4 NREL, Best research-cell efficiencies chart. https://www.nrel.gov/pv/cell-efficiency.html.(20210104).pdf.
5 N. K. Noel, S. N. Habisreutinger, A. Pellaroque, F. Pulvirenti, B. Wenger, F. Zhang, Y.-H. Lin, O. G. Reid, J. Leisen, Y. Zhang, S. Barlow, S. R. Marder, A. Kahn, H. J. Snaith, C. B. Arnold and B. P. Rand, Interfacial charge-transfer doping of metal halide perovskites for high performance photovoltaics, *Energy Environ. Sci.*, 2019, **12**, 3063–3073.
6 F. Hao, C. C. Stoumpos, D. H. Cao, R. P. H. Chang and M. G. Kanatzidis, Lead-free solid-state organic–inorganic halide perovskite solar cells, *Nat. Photonics*, 2014, **8**, 489–494.
7 W.-H. Chen, L. Qiu, P. Zhang, P.-C. Jiang, P. Du, L. Song, J. Xiong and F. Ko, Simple fabrication of a highly conductive and passivated PEDOT:PSS film via cryo-controlled quasi-congealing spin-coating for flexible perovskite solar cells, *J. Mater. Chem. C*, 2019, **7**, 10247–10256.
8 S. Bag and M. F. Durstock, Efficient semi-transparent planar perovskite solar cells using a 'molecular glue', *Nano Energy*, 2016, **30**, 542–548.
9 D. Wang, C. Wu, W. Luo, X. Guo, X. Qi, Y. Zhang, Z. Zhang, B. Qu, L. Xiao and Z. Chen, Glass rod-sliding and low pressure assisted solution processing composition engineering for high-efficiency perovskite solar cells, *Sol. Energy Mater. Sol. Cells*, 2020, **211**, 110532.
10 D. Chi, S. Huang, M. Zhang, S. Mu, Y. Zhao, Y. Chen and J. You, Composition and Interface Engineering for Efficient and Thermally Stable Pb-Sn Mixed Low-Bandgap Perovskite Solar Cells, *Adv. Funct. Mater.*, 2018, **28**, 1804603.
11 X. Guo, B. Zhang, Z. Lin, J. Ma, J. Su, W. Zhu, C. Zhang, J. Zhang, J. Chang and Y. Hao, Interface engineering of

TiO_2/perovskite interface via fullerene derivatives for high performance planar perovskite solar cells, *Org. Electron.*, 2018, **62**, 459–467.

12 A. Agresti, A. Pazniak, S. Pescetelli, A. Di Vito, D. Rossi, A. Pecchia, M. Auf der Maur, A. Liedl, R. Larciprete, D. V. Kuznetsov, D. Saranin and A. Di Carlo, Titanium-carbide MXenes for work function and interface engineering in perovskite solar cells, *Nat. Mater.*, 2019, **18**, 1228–1234.

13 H. Chen, Q. Luo, T. Liu, J. Ren, S. Li, M. Tai, H. Lin, H. He, J. Wang and N. Wang, Goethite Quantum Dots as Multifunctional Additives for Highly Efficient and Stable Perovskite Solar Cells, *Small*, 2019, **15**, e1904372.

14 P. Wang, Q. Jiang, Y. Zhao, Y. Chen, Z. Chu, X. Zhang, Y. Zhou and J. You, Synergistic improvement of perovskite film quality for efficient solar cells via multiple chloride salt additives, *Sci. Bull.*, 2018, **63**, 726–731.

15 X. He, J. Wu, T. Wu, Z. Lan and M. Huang, Dimethyl Sulfoxide Solvent Engineering for High Quality Cation-Anion-Mixed Hybrid and High Efficiency Perovskite Solar Cells, *Energy Technol.*, 2019, **7**, 346–351.

16 T. Bu, L. Wu, X. Liu, X. Yang, P. Zhou, X. Yu, T. Qin, J. Shi, S. Wang, S. Li, Z. Ku, Y. Peng, F. Huang, Q. Meng, Y.-B. Cheng and J. Zhong, Synergic Interface Optimization with Green Solvent Engineering in Mixed Perovskite Solar Cells, *Adv. Energy Mater.*, 2017, **7**, 1700576.

17 N. K. Noel, A. Abate, S. D. Stranks, E. S. Parrott, V. M. Burlakov, A. Goriely and H. J. Snaith, Enhanced Photoluminescence and Solar Cell Performance via Lewis Base Passivation of OrganicInorganic Lead Halide Perovskites, *ACS Nano*, 2014, **8**, 9815–9821.

18 S. Yang, S. Chen, E. Mosconi, Y. Fang, X. Xiao, C. Wang, Y. Zhou, Z. Yu, J. Zhao, Y. Gao, F. D. Angelis and J. Huang, Stabilizing halide perovskite surfaces for solar cell operation with wide-bandgap lead oxysalts, *Science*, 2019, **365**, 473–478.

19 C. Xu, Z. Liu and E.-C. Lee, Crystallization management for high-performance perovskite solar cells by introducing an antisolvent into the perovskite precursor, *J. Mater. Chem. C*, 2020, **8**, 15860–15867.

20 Y. Li, L. Li, A. S. Yerramilli, Y. Chen, D. Fang, Y. Shen and T. L. Alford, Enhanced power conversion efficiency and preferential orientation of the $MAPbI_3$ perovskite solar cells by introduction of urea as additive, *Org. Electron.*, 2019, **73**, 130–136.

21 W. Zhang, Y. Li, X. Liu, D. Tang, X. Li and X. Yuan, Ethyl acetate green antisolvent process for high-performance planar low-temperature SnO_2-based perovskite solar cells made in ambient air, *Chem. Eng. J.*, 2020, **379**, 122298.

22 X. Sun, D. Zhao and Z. Li, Recent advances in the design of dopant-free hole transporting materials for highly efficient perovskite solar cells, *Chin. Chem. Lett.*, 2018, **29**, 219–231.

23 M. Kong, H. Hu, K. Egbo, B. Dong, L. Wan and S. Wang, Anti-solvent assisted treatment for improved morphology and efficiency of lead acetate derived perovskite solar cells, *Chin. Chem. Lett.*, 2019, **30**, 1325–1328.

24 J. Yang, S. Xiong, T. Qu, Y. Zhang, X. He, X. Guo, Q. Zhao, S. Braun, J. Chen, J. Xu, Y. Li, X. Liu, C. Duan, J. Tang, M. Fahlman and Q. Bao, Extremely Low-Cost and Green Cellulose Passivating Perovskites for Stable and High-Performance Solar Cells, *ACS Appl. Mater. Interfaces*, 2019, **11**, 13491–13498.

25 B. S. Fales, N. O. Fujamade, Y. w. Nei, J. Oomens and M. T. Rodgers, Infrared Multiple Photon Dissociation Action Spectroscopy and Theoretical Studies of Diethyl Phosphate Complexes: Effects of Protonation and Sodium Cationization on Structure, *J. Am. Soc. Mass Spectrom.*, 2011, **22**, 81–92.

26 H. Shahivandi, M. Vaezzadeh and M. Saeidi, Iodine Vacancy Formation Energy in $CH_3NH_3PbI_3$ Perovskite, *IEEE J. Photovolt.*, 2020, **10**, 1750–1756.

27 N. De Marco, H. Zhou, Q. Chen, P. Sun, Z. Liu, L. Meng, E.-P. Yao, Y. Liu, A. Schiffer and Y. Yang, Guanidinium: A Route to Enhanced Carrier Lifetime and Open-Circuit Voltage in Hybrid Perovskite Solar Cells, *Nano Lett.*, 2016, **16**, 1009–1016.

28 S. Bae, J. W. Jo, P. Lee and M. J. Ko, Controlling the Morphology of Organic-Inorganic Hybrid Perovskites through Dual Additive-Mediated Crystallization for Solar Cell Applications, *ACS Appl. Mater. Interfaces*, 2019, **11**, 17452–17458.

29 Y. Liu, J. Duan, J. Zhang, S. Huang, W. Ou-Yang, Q. Bao, Z. Sun and X. Chen, High Efficiency and Stability of Inverted Perovskite Solar Cells Using Phenethyl Ammonium Iodide-Modified Interface of NiOx and Perovskite Layers, *ACS Appl. Mater. Interfaces*, 2020, **12**, 771–779.

30 X. Zhao, C. Yao, T. Liu, J. C. Hamill Jr., G. O. Ngongang Ndjawa, G. Cheng, N. Yao, H. Meng and Y. L. Loo, Extending the Photovoltaic Response of Perovskite Solar Cells into the Near-Infrared with a Narrow-Bandgap Organic Semiconductor, *Adv. Mater.*, 2019, **31**, e1904494.

31 W. Zhou, D. Li, Z. Xiao, Z. Wen, M. Zhang, W. Hu, X. Wu, M. Wang, W. H. Zhang, Y. Lu, S. Yang and S. Yang, Zwitterion Coordination Induced Highly Orientational Order of $CH_3NH_3PbI_3$ Perovskite Film Delivers a High Open Circuit Voltage Exceeding 1.2 V, *Adv. Funct. Mater.*, 2019, **29**, 1901026.

32 D. Bi, C. Yi, J. Luo, J.-D. Décoppet, F. Zhang, S. M. Zakeeruddin, X. Li, A. Hagfeldt and M. Grätzel, Polymer-templated nucleation and crystal growth of perovskite films for solar cells with efficiency greater than 21%, *Nat. Energy*, 2016, **1**, 16142.

33 J. Zhu, B. He, Z. Gong, Y. Ding, W. Zhang, X. Li, Z. Zong, H. Chen and Q. Tang, Grain Enlargement and Defect Passivation with Melamine Additives for High Efficiency and Stable CsPbBr3 Perovskite Solar Cells, *ChemSusChem*, 2020, **13**, 1834–1843.

34 G. Sadoughi, D. E. Starr, E. Handick, S. D. Stranks, M. Gorgoi, R. G. Wilks, M. Bär and H. J. Snaith, Observation and Mediation of the Presence of Metallic Lead in Organic–Inorganic Perovskite Films, *ACS Appl. Mater. Interfaces*, 2015, **7**, 13440–13444.

35 N. Chen, X. Yi, J. Zhuang, Y. Wei, Y. Zhang, F. Wang, S. Cao, C. Li and J. Wang, An Efficient Trap Passivator for Perovskite Solar Cells: Poly(propylene glycol) bis(2-aminopropyl ether), *Nano-Micro Lett.*, 2020, **12**, 177.

36 J. D. McGettrick, K. Hooper, A. Pockett, J. Baker, J. Troughton, M. Carnie and T. Watson, Sources of Pb(0) artefacts during XPS analysis of lead halide perovskites, *Mater. Lett.*, 2019, **251**, 98–101.

37 W. Li, X. Lai, F. Meng, G. Li, K. Wang, A. K. K. Kyaw and X. W. Sun, Efficient defect-passivation and charge-transfer with interfacial organophosphorus ligand modification for enhanced performance of perovskite solar cells, *Sol. Energy Mater. Sol. Cells*, 2020, **211**, 110527.

38 N. K. Tailor, M. Abdi-Jalebi, V. Gupta, H. Hu, M. I. Dar, G. Li and S. Satapathi, Recent progress in morphology optimization in perovskite solar cell, *J. Mater. Chem. A*, 2020, **8**, 21356–21386.

39 J. Zhang, T. Tong, L. Zhang, X. Li, H. Zou and J. Yu, Enhanced Performance of Planar Perovskite Solar Cell by Graphene Quantum Dot Modification, *ACS Sustainable Chem. Eng.*, 2018, **6**, 8631–8640.

40 M. Kim, S. G. Motti, R. Sorrentino and A. Petrozza, Enhanced solar cell stability by hygroscopic polymer passivation of metal halide perovskite thin film, *Energy Environ. Sci.*, 2018, **11**, 2609–2619.

41 Y. Cai, J. Cui, M. Chen, M. Zhang, Y. Han, F. Qian, H. Zhao, S. Yang, Z. Yang, H. Bian, T. Wang, K. Guo, M. Cai, S. Dai, Z. Liu and S. Liu, Multifunctional Enhancement for Highly Stable and Efficient Perovskite Solar Cells, *Adv. Funct. Mater.*, 2020, 2005776.

42 M. Wang, B. Li, P. Siffalovic, L.-C. Chen, G. Cao and J. Tian, Monolayer-like hybrid halide perovskite films prepared by additive engineering without antisolvents for solar cells, *J. Mater. Chem. A*, 2018, **6**, 15386–15394.

43 Y. Yang, Y. Yan, M. Yang, S. Choi, K. Zhu, J. M. Luther and M. C. Beard, Low surface recombination velocity in solution-grown $CH_3NH_3PbBr_3$ perovskite single crystal, *Nat. Commun.*, 2015, **6**, 7961.

44 Q. Zeng, X. Zhang, X. Feng, S. Lu, Z. Chen, X. Yong, S. A. T. Redfern, H. Wei, H. Wang, H. Shen, W. Zhang, W. Zheng, H. Zhang, J. S. Tse and B. Yang, Polymer-Passivated Inorganic Cesium Lead Mixed-Halide Perovskites for Stable and Efficient Solar Cells with High Open-Circuit Voltage over 1.3 V, *Adv. Mater.*, 2018, **30**, 1705393.

45 F. Wu, R. Pathak, K. Chen, G. Wang, B. Bahrami, W.-H. Zhang and Q. Qiao, Inverted Current–Voltage Hysteresis in Perovskite Solar Cells, *ACS Energy Lett.*, 2018, **3**, 2457–2460.

46 T. Bu, X. Liu, Y. Zhou, J. Yi, X. Huang, L. Luo, J. Xiao, Z. Ku, Y. Peng, F. Huang, Y.-B. Cheng and J. Zhong, A novel quadruple-cation absorber for universal hysteresis elimination for high efficiency and stable perovskite solar cells, *Energy Environ. Sci.*, 2017, **10**, 2509–2515.

47 R. Wang, K. Jiang, H. Yu, F. Wu, L. Zhu and H. Yan, Efficient inverted perovskite solar cells with truxene-bridged PDI trimers as electron transporting materials, *Mater. Chem. Front.*, 2019, **3**, 2137–2142.

48 Y. Liu, Z. Liu and E.-C. Lee, Dimethyl-sulfoxide-assisted improvement in the crystallization of lead-acetate-based perovskites for high-performance solar cells, *J. Mater. Chem. C*, 2018, **6**, 6705–6713.

49 X. Zhou, C. Xin, F. Hou, B. Shi, S. Pan, S. Hou, J. Zhang, P. Wang, H. Ren, Y. Zhao, G. Wang, Y. Li and X. Zhang, Role of Moisture in the Preparation of Efficient Planar Perovskite Solar Cells, *ACS Sustainable Chem. Eng.*, 2019, **7**, 17691–17696.

50 M. Wang, B. Li, P. Siffalovic, L.-C. Chen, G. Cao and J. Tian, Monolayer-like hybrid halide perovskite films prepared by additive engineering without antisolvents for solar cells, *J. Mater. Chem. A*, 2018, **6**, 15386–15394.

51 Z. Ye, J. Zhou, J. Hou, F. Deng, Y.-Z. Zheng and X. Tao, Low Temperature-Processed Stable and Efficient Carbon-Based $CsPbI_2Br$ Planar Perovskite Solar Cells by In Situ Passivating Grain Boundary and Trap Density, *Sol. RRL*, 2019, **3**, 1900109.

52 J. Shao, X. Guo, N. Shi, X. Zhang, S. Liu, Z. Lin, B. Zhao, J. Chang, J. Shao and X. Dong, Acenaphthylene-imide based small molecules/TiO_2 bilayer as electron-transporting layer for solution-processing efficient perovskite solar cells, *Sci. China Mater.*, 2018, **62**, 497–507.

53 S. Kundu and T. L. Kelly, Improving the moisture stability of perovskite solar cells by using PMMA/P3HT based hole-transport layers, *Mater. Chem. Front.*, 2018, **2**, 81–89.

54 L. Xie, K. Lin, J. Lu, W. Feng, P. Song, C. Yan, K. Liu, L. Shen, C. Tian and Z. Wei, Efficient and Stable Low-Bandgap Perovskite Solar Cells Enabled by a $CsPbBr_3$-Cluster Assisted Bottom-up Crystallization Approach, *J. Am. Chem. Soc.*, 2019, **141**, 20537–20546.